Hindawi
Shock and Vibration
Volume 2023, Article ID 4351878, 17 pages
https://doi.org/10.1155/2023/4351878

Research Article

Dynamic Response and Parameter Analysis of Electromagnetic Railguns under Time Varying Moving Loads

Lilan Liu,[1] **Xukai Zhang**,[2] **and Jiayi Wang**[1]

[1]*Xi'an University of Technology, Xi'an, China*
[2]*Yangling Vocational and Technical College, Xi'an, China*

Correspondence should be addressed to Lilan Liu; liulilans@163.com

Received 19 September 2023; Revised 28 November 2023; Accepted 1 December 2023; Published 19 December 2023

Academic Editor: Traian Mazilu

During the launch process of an electromagnetic railgun, the armature is subjected to the ampere force and moves along the rail with variable acceleration. In this period, the rail is excited by time varying moving loads and generates lateral vibration. For analysis, the rail is simplified as an Euler–Bernoulli beam, and the nonlinear dynamic equation of the beam under time varying moving loads is established. The electromagnetic repulsive force between rails, the contact pressure between the armature and the rail, and the thermal expansion pressure acting on the rail are taken into account. The lateral vibration response of the rail is achieved by using the analytical method combined with numerical integration. The variable motion of the armature during launch is also illustrated. Furthermore, the study of the effects of structure parameters on the vibration amplitude of the rail is performed. The research results can provide a theoretical basis for the structural optimization and vibration reduction of electromagnetic railguns.

1. Introduction

Electromagnetic (EM) launch technology is a revolution in the launch mode which uses EM energy to propel objects to high speed or even ultrahigh speed [1]. EM railguns are the most important application of the EM launch technology, which have many advantages such as high speed, long range, and strong power [2]. As one of the newest powerful weapons, EM railguns have attracted great attention in military field in recent years, especially in America, Russia, and China [3–5].

During the launch process, the armature moves along the rails of EM railguns under the action of the ampere force generated by the heavy current. Meanwhile, the rail is subjected to moving loads which will result in its nonlinear lateral vibration. Rail vibration can affect the contact status and shot accuracy, even causing damage between the armature and the rail [6]. In order to ensure the launch accuracy and reliability of EM railguns, it is necessary to analyze the vibration response of the rail.

A typical barrel of EM railguns is mainly composed of two rails, elastic insulation layers, and the containment structure with fastening parts. When the out containment is assumed to be a rigid boundary and the insulation layer is an elastic support, the rail can be seen as a beam on an elastic base [7]. Therefore, many works established a beam model sitting on an elastic foundation to analyze the vibration of the rail. Tzeng [8] simplified the rail of EM railguns as a Timoshenko beam founded on an elastic base. The influences of design parameters and material characteristics on the critical velocity of the rail were analyzed. Johnson and Moon [9] adopted a finite element code to calculate the dynamic deflection of the rail which was simplified as a Timoshenko beam. Simulation results showed that the contact pressure between the armature and the rail changes when the speed of the armature reaches the critical velocity of the rail. In addition, Nechitailo and Lewis [10, 11] modeled an Euler–Bernoulli beam subjected to uniform pressure to estimate the critical velocity of the rail. Numerical tests using the finite element analysis were used to illustrate the existence of the group resonance phenomenon. Daneshjoo et al. [12] built an Euler–Bernoulli beam model of the rail to study its dynamic behavior. Results showed that the resulting maximum deflection varies with physical and

mechanical parameters of the rail. However, these results are mainly applicable to the analysis of the critical velocity and resonance in a hypervelocity launcher, always assuming constant pressure on the rail as well as constant speed of the armature.

To analyze the dynamic response of the rail, many approaches have been presented. Yang et al. [13] studied the contact between the armature and the rail during launch by a finite element model with LS-DYNA code. Three types of C-shaped armatures were designed to match rails with curvatures. Reck et al. [14] also used the LS-DYNA code to simulate a projectile launch with a moving armature. Assuming the pressure acting on the rail is uniform, the dynamic deformations of the rail and the dynamic stress states were studied. Chen et al. [15] applied the numerical analysis methods to obtain the dynamic response of the rail. The actions of the EM repulsion and the thermal expansion pressure of the armature were considered. Tian et al. [16] simplified the rail as a beam on an elastic foundation. The dynamic response of the beam was solved by using two-dimensional Fourier integral transformation. Yin et al. [17] calculated the critical velocity of a flexural wave in the composite housing of the railgun barrel using the 3D transient finite element. The dynamic responses and the development of damage for the railgun barrel were analyzed. Zhang et al. [18] also treated the rail as an Euler–Bernoulli beam and proposed a nonlinear finite element model to study the dynamic characteristics of the rail. In the work, the repulsive force and the contact pressure acting on the rail were considered.

As we know, the dynamics of beams under moving loads has been widely studied for their extensive applications in engineering, such as railroads, bridges, and transport pipelines. The research procedures on beams can provide helpful ideas for solving the dynamic equation of the rail under time varying moving loads in this paper. Based on the references we have found, there are two types of moving loads on beams which are mainly studied. One is a single moving load, and the other is a harmonic moving load. On the aspect of a single moving load, for instance, AlSaleh et al. [19] investigated the dynamic response of Euler–Bernoulli beams under a traversing moving load based on Green's functions combined with a decomposition technique. The load was assumed to be moving with different values of constant velocity. Akbas et al. [20] analyzed the vibration of a simply supported porous microbeam made of functionally graded materials subjected to a moving load. The governing equations were obtained by the Lagrange procedure and were solved by Ritz and Newmark average acceleration methods. And then, they also studied the dynamics of carbon nanotube-reinforced composite beams under a moving load using the same methods [21]. Guo et al. [22] studied the forced vibration response of thick microplates under a moving load with acceleration in speed on its upper surface. The governing equations for simply supported microplate were solved by developing a state space method in conjunction with a set of mathematical series. Bozyigit [23] proposed an analytical method based on a combination of transfer matrix formulations and modal superposition to obtain the forced vibration of damaged beams subjected to a moving concentrated load. Kumar et al. [24] derived a simple closed-form expression for free vibration response, and the dynamic behavior of simply supported uniform beams subjected to a single moving point load was analyzed. Moreover, Esen [25] investigated the forced vibration of microbeams under a moving point load with constant velocity using the Newmark-β method and the finite element method. For the case of a harmonic moving load, Eyvazian et al. [26] investigated the dynamic analysis of a composite cylindrical nanoshell on an elastic foundation subjected to a moving harmonic load. The equations of motion were derived based on first-order shear deformation theory and the nonlocal strain gradient theory. Kim and Cho [27] investigated the vibration and buckling of an infinite shear beam-column resting on an elastic foundation. The response of the beam under moving harmonic loads was obtained using a Fourier transform. Yang et al. [28] established the governing equation of a simply supported thin-walled beam under a harmonic moving load, and closed-form solutions were presented for the lateral, vertical, and torsional vibration of the beam. Chen et al. [29] studied the responses of an infinite beam resting on a tensionless viscoelastic foundation under a harmonic point force moving with a constant speed. To solve the governing equation, the infinite beam is replaced by a finite long beam expanding the beam deflection into a harmonic series. In addition, in the study of dynamic behaviors of the beam supported on a viscoelastic foundation. Bozyigit et al. [30] developed a comprehensive method to solve the motion equations by combing the Adomian decomposition method and the differential transform method.

In terms of EM railguns, the existing research works provide a good foundation for the vibration analysis and structural design of rails. However, most results are applicable to constant pressure or constant speed of armature motion. In fact, since the exciting current is changing with time, the armature undergoes a variable acceleration motion along the rail. The dynamic response of beams is significantly affected by varying the moving velocity of loads [19]. In this paper, in order to study the dynamic behavior of EM railguns deeply, more consideration is given on the nonuniform motion of the armature and the moving loads on rail. Three kinds of forces acting on the rail are involved, which are time varying and nonperiod, more complex than the constant and periodic moving loads. The dynamic governing equation of an Euler–Bernoulli beam under time varying moving loads is established. Due to its high nonlinearity, an analytical method combined with numerical integration is presented to get solutions of the governing equation. The lateral vibration response of the rail in the process of launching is achieved. Furthermore, the influences of parameters on the vibration amplitude of the rail are analyzed. The results obtained can provide a meaningful tool for the vibration analysis of EM railguns.

2. Dynamic Modeling of the Rail

2.1. Mathematical Model. The schematic diagram of the barrel of an EM railgun is shown in Figure 1, which is mainly composed of two rails, an armature, elastic insulation layers,

and the containment structure which includes the stiffening steel plates and steel bolts. During launch, the current flows in from one rail through the armature and then out from the other rail, as shown in Figure 2. The current generates a strong magnetic field between the two rails, and so the armature moves along the rails propelled by the ampere force. In addition, when the armature is sliding, friction exists between the armature and the rail.

The rail has a rectangular cross section and has a large slenderness ratio. During launch, the rail mainly bears lateral loads perpendicular to the axial. Assuming that the cross section is always perpendicular to the axis when the lateral vibration of the beam occurs, the rail can be simplified as an Euler–Bernoulli beam with an elastic insulation support wrapped in a rigid constraint, as shown in Figure 3. In addition, the insulation layer is thin and the outer containment is rigid. Under these conditions, the elastic support behavior is similar to the spring model. Therefore, the elastic foundation of the rail is modeled as a Winkler foundation model ignoring the shear deflection. The Winkler model has a simple form and is mathematically easy to handle, and it is used popularly in the analysis of EM railguns in most previous studies [9–16].

To improve the stability and life of the barrel of EM railguns, the insulation should use materials with sufficient strength and stiffness to bear the forces transmitted from the rail. The greater the stiffness of the insulation gets, the smaller the effect of its damping is. Therefore, most studies ignore the damping in modeling for simplification [6–18].

The governing equation of the beam subjected to the time varying moving load is established as follows [7]:

$$\mathrm{EI}\frac{\partial^4 \omega(x,t)}{\partial x^4} + m\frac{\partial^2 \omega(x,t)}{\partial t^2} + k\omega(x,t) = q(x,t), \quad (1)$$

where $\omega(x, t)$ is the lateral vibration amplitude of the rail, E is the modulus of rail material, I is the moment of inertia of the cross section, m is the mass per unit length of rail, k is the elastic foundation coefficient, and $q(x, t)$ represents the time varying moving load.

When the armature moves along the rail at ultrahigh speed, the rail suffers moving loads. In many studies, to obtain the critical velocity of rail, only the EM repulsive force on rail is considered [7–12]. With further researches, Cao et al. [31] established the governing equation of an Euler–Bernoulli beam under moving loads to investigate the dynamic response of the rail. In the study, two forces including the repulsive force between rails and the thermal pressure of armature on rail were considered. Wu et al. [32] also simplified the rail to an Euler–Bernoulli beam supported by an elastic base to analyze the vibration response of the rail. In the work, the repulsive force and the contact pressure acting on the rail were considered. Based on the above works, we believe that there are three kinds of forces acting on the rail actually; i.e., the EM repulsive force between rails, the contact pressure between the armature and the rail due to factors such as preloading for tight fitting, and the thermal expansion pressure of the armature induced by the Joule heating effect, respectively.

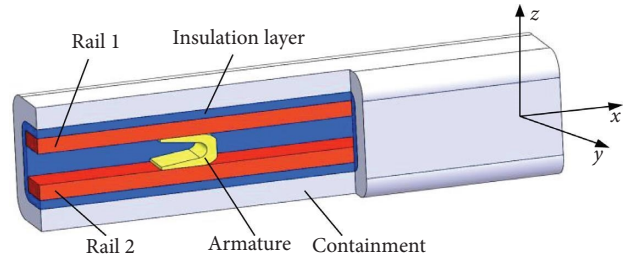

Figure 1: Schematic diagram of the barrel of an EM railgun.

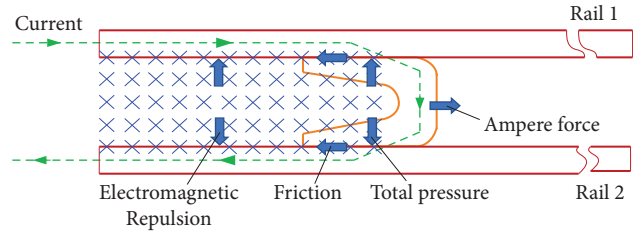

Figure 2: Schematic diagram of forces acting on the rail and armature.

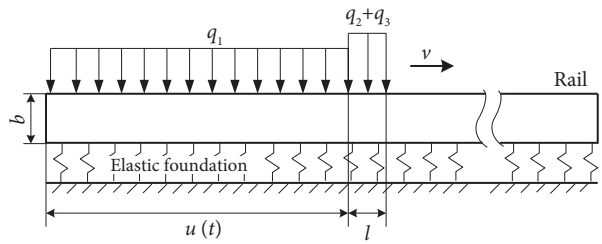

Figure 3: Beam model of the rail.

Therefore, the time varying moving loads on rail are composed of three parts as follows:

$$q(x,t) = q_1(t)[1 - H(x - u(t))] + (q_2(t) + q_3(t))H\left[\left(\frac{1}{2}l\right)^2 - (x - u(t))^2\right], \quad (2)$$

where $q_1(t)$, $q_2(t)$, and $q_3(t)$ are the EM repulsive force, the contact pressure, and the thermal expansion pressure, respectively, H is a Heaviside step function, $u(t)$ is the displacement of the armature, and l is the contact length between the armature and the rail.

2.2. Loads Computation

2.2.1. EM Repulsive Force. The EM field coordinate of the rail is established as shown in Figure 4. Considering the skin effect of the current and ignoring the distribution of current in the width direction of the rail, the magnetic induction intensity at any point between two rails can be obtained.

According to the Biot–Savart law and reference [33], the magnetic induction intensity B generated by rail 1 at the infinitesimal dy' of rail 2 is as follows:

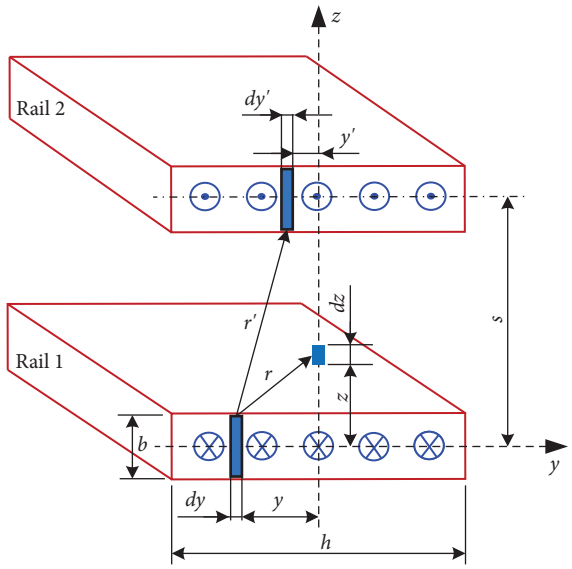

Figure 4: Coordinate system of the EM field.

$$B = \frac{\mu_0}{4\pi}\int_{-h/2}^{h/2}\frac{(i(t)/h)\mathrm{d}y}{s^2+\left(y-y'\right)^2} = \frac{\mu_0 i(t)}{4\pi h s}\left[\arctan\frac{h/2-y'}{s}+\arctan\frac{h/2+y'}{s}\right], \tag{3}$$

where μ_0 is the vacuum permeability, h *is* the height of the rail, s is the distance between the inner walls of two rails, and $i(t)$ is the current.

Therefore, the EM repulsive force q_1 between rail 1 and rail 2 is derived as follows:

$$q_1 = \int_{-h/2}^{h/2} B\frac{i(t)}{h}\mathrm{d}y' = \frac{\mu_0 i^2(t)}{4\pi h^2 s}\left[2h\arctan\frac{h}{s}+s\ln\frac{s^2}{s^2+h^2}\right]. \tag{4}$$

2.2.2. Contact Pressure. In order to avoid the occurrence of transition and ensure steady contact between the armature and the rail, the Anker law is usually used to judge whether the contact pressure provided by the tight fit can meet the launch demand. However, when the armature moves along the rail at a superhigh speed, the contact pressure will be impacted by the initial interference between the armature and the rail and the tension of the armature under the action of current as well as the wear of the armature [34]. So, the calculation of the contact pressure q_2 is complex to some extent.

The contact pressure can be approximately calculated by the following equation [31]:

$$q_2 = \frac{L' l i^2(t)}{s^2}, \tag{5}$$

where L' is the inductance gradient. The calculation method of L' is detailed in reference [35].

2.2.3. Thermal Expansion Pressure. When the current passes through the armature, the armature will inevitably generate a large amount of heat inside it because of the Joule heating effect. The Joule heat will cause thermal expansion of the armature and therefore produce a thermal expansion pressure on the rail. According to references [31, 36], assuming that the current inside the armature distributes uniformly, the temperature distribution of the armature along its height direction is computed by the following equation:

$$T_d = T_f + \frac{P(t)h^2}{8\lambda_T}\left[1+\frac{4\lambda_T}{h\alpha_F}-4\left(\frac{y}{h_a}\right)^2\right], \tag{6}$$

where h_a is the height of the armature, α_F is the heat transfer coefficient of armature material, T_f is the temperature of the medium adjacent to the armature, λ_T is the thermal conductivity coefficient of armature material, σ_d is the conductivity of armature material, and $P(t) = 0.86(J^2(t)/\sigma_d)$ is the power of the Joule heat with the current density $J(t) = (i(t)/l{\cdot}h_a)$.

Given an extremely short acting time, the change of the temperature can be ignored. The average temperature along the height direction of the armature is taken as the basis for calculation. Based on equation (6), ignoring the medium temperature, the thermal strain of the armature is obtained as follows:

$$\varepsilon_T(t) = \frac{\alpha_T}{h_a}\int_{-h_a/2}^{h_a/2} T_d\mathrm{d}y = \frac{P(t)h_a\alpha_T}{8}\left[\frac{4\lambda_T}{\alpha_F}+\frac{2}{3}h_a\right], \tag{7}$$

where α_T is the linear expansion coefficient of armature material.

Therefore, assuming that the armature expands uniformly and the force acting on the rail is even, the thermal expansion pressure of the armature on rail is derived as follows:

$$q_3 = \varepsilon_T(t)E_d h_a l = \frac{E_d P(t){h_a}^2 l\alpha_T}{8}\left[\frac{4\lambda_T}{\alpha_F}+\frac{2}{3}h_a\right], \tag{8}$$

where E_d is the elastic modulus of armature material.

3. Movement of the Armature

As shown in Figure 4, according to the Biot–Savart law, the magnetic induction intensity B_1 generated by rail 1 at the infinitesimal dz is as follows:

$$B_1 = \frac{\mu_0}{4\pi}\int_{-h/2}^{h/2}\frac{(i(t)/h)}{z^2+y^2}\mathrm{d}y = \frac{\mu_0 i(t)}{2\pi h z}\arctan\frac{h}{2z}. \tag{9}$$

Similarly, the magnetic induction intensity B_2 generated by rail 2 at the infinitesimal dz is as follows:

$$B_2 = \frac{\mu_0 i(t)}{2\pi h(s-z)}\arctan\frac{h}{2(s-z)}. \tag{10}$$

Thus, the Ampere force on the armature is calculated by the following equation:

$$F = \int_0^s (B_1 + B_2) i(t) \mathrm{d}z. \tag{11}$$

In addition, there is friction between the armature and the rail. Ignoring the static friction at the initial startup stage, the thrust force of the armature in the sliding stage is as follows:

$$F_a = F - F_f = F - 2\mu F_N, \tag{12}$$

where F_f is the friction force, μ is the coefficient of sliding friction, and $F_N = (q_2 + q_3)hl$ is the normal pressure.

Therefore, according to the Newton's second law, the velocity and displacement of the armature during launch can be derived as follows:

$$\begin{aligned} v(t) &= \int_0^t \frac{F_a}{M} \mathrm{d}t = \int_0^t \frac{F - 2\mu F_N}{M} \mathrm{d}t, \\ u(t) &= u_0 + \int_0^t v(t) \mathrm{d}t = u_0 + \int_0^t \int_0^t \frac{F - 2\mu F_N}{M} \mathrm{d}t \mathrm{d}t, \end{aligned} \tag{13}$$

where M and u_0 are the mass and the initial position of the armature, respectively.

4. Solving Method

Here, the method of separation of variables is adopted to solve the differential equation of the rail. The solution of equation (1) is assumed as follows [19]:

$$\omega(x,t) = \theta(x)\varphi(t) = \sum_{i=1}^{\infty} \theta_i(x)\varphi_i(t), \tag{14}$$

where $\theta(x)$ and $\phi(t)$ represent the vibration mode and the vibration rule, respectively.

The homogeneous vibration equation of equation (1) is as follows:

$$\mathrm{EI} \frac{\partial^4 \omega(x,t)}{\partial x^4} + m \frac{\partial^2 \omega(x,t)}{\partial t^2} + k\omega(x,t) = 0. \tag{15}$$

Substituting equation (14) into equation (15), there is

$$\mathrm{EI}\varphi(t) \frac{\partial^4 \theta(x)}{\partial x^4} + m\theta(x) \frac{\partial^2 \varphi(t)}{\partial t^2} + k\theta(x)\varphi(t) = 0. \tag{16}$$

Equation (16) can also be expressed as follows:

$$\frac{\mathrm{EI}}{m} \frac{\left(d^4\theta(x)/\mathrm{d}x^4\right)}{\theta(x)} + \frac{k}{m} = -\frac{\left(d^2\phi(t)/\mathrm{d}t^2\right)}{\phi(t)}. \tag{17}$$

In equation (17), x and t are independent of each other. So, both sides of the equation must be a constant at the same time, and the constant should be nonnegative. Assuming the constant is γ^2, equation (17) is transformed into the following two independent equations:

$$\begin{cases} \dfrac{d^4\theta(x)}{dx^4} - \delta^4\theta(x) = 0, \\ \dfrac{d^2\phi(t)}{dt^2} + \gamma^2\phi(t) = 0, \end{cases} \tag{18}$$

with

$$\delta^4 = \frac{m\left(\gamma^2 - (/)\right)}{EI}. \tag{19}$$

Now, solutions of equation (18) can be expressed as follows:

$$\begin{cases} \theta(x) = a_1 e^{\delta x} + a_2 e^{-\delta x} + a_3 \sin \delta x + a_4 \cos \delta x, \\ \phi(t) = c_1 \cos \gamma t + c_2 \sin \gamma t. \end{cases} \tag{20}$$

Introducing hyperbolic functions, i.e., $\cosh x = (e^x + e^{-x})/2$ and $\sinh x = (e^x - e^{-x})/2$ into equation (20), the solutions of equation (18) are rewritten as follows:

$$\begin{cases} \theta(x) = a_1 \sinh \delta x + a_2 \cosh \delta x + a_3 \sin \delta x + a_4 \cos \delta x, \\ \phi(t) = c_1 \cos \gamma t + c_2 \sin \gamma t, \end{cases} \tag{21}$$

where a_1, a_2, a_3, and a_4 are constant coefficients which can be determined by the boundary conditions and the initial conditions, c_1 and c_2, are constant coefficients.

According to Appendix A, the constant coefficients a_1, a_2, a_3, and a_4 can be obtained. Substituting equation (A.7) into equation (21), the ith-order vibration mode of the rail $\theta_i(x)$ is derived as follows:

$$\begin{aligned} \theta_i(x) &= \left(\cosh \delta_i x - \cos \delta_i x\right) \\ &\quad - \frac{\sinh \delta_i L - \sin \delta_i L}{\cosh \delta_i L + \cos \delta_i L} \left(\sinh \delta_i x - \sin \delta_i x\right). \end{aligned} \tag{22}$$

The function $\theta_i(x)$ is an orthogonal function which satisfies the following formula:

$$\int_0^L \theta_i(x)\theta_j(x) \mathrm{d}x = \begin{cases} 0, & i \neq j, \\ 1, & i = j. \end{cases} \tag{23}$$

Next, in order to obtain $\phi(t)$ in equation (14) under the time varying moving load $q(x, t)$, the Lagrange equation of the rail is established as follows [37]:

$$\frac{d}{dt}\left(\frac{\partial T}{\partial(d\phi(t)/dt)}\right) - \frac{\partial T}{\partial \phi(t)} + \frac{\partial U}{\partial \phi(t)} = Q(t), \tag{24}$$

where T and U are the kinetic energy and the total potential energy of the beam, respectively. Also, $Q(t)$ is a generalized force, which is defined as follows:

$$Q(t) = \int_0^L q(x,t)\theta(x)dx. \tag{25}$$

According to Appendix B, the kinetic energy T and the total potential energy U of the beam can be obtained. So, based on equations (B.3) and (B.7), the following equations are obtained:

$$\begin{aligned}\frac{d}{dt}\left(\frac{\partial T}{\partial(d\phi(t)/dt)}\right) &= \frac{d}{dt}\left(\frac{\partial\left(1/2\sum_i M_i\left(d\phi_i(t)/dt\right)^2\right)}{\partial(d\phi(t)/dt)}\right)\\ &= \sum_i M_i\frac{d^2\phi_i(t)}{dt^2},\end{aligned} \tag{26}$$

$$\frac{\partial T}{\partial\phi(t)} = 0, \tag{27}$$

$$\frac{\partial U}{\partial\phi(t)} = \frac{\partial\left(1/2\sum_i M_i{\phi_i}^2(t)\gamma_i^2\right)}{\partial\phi(t)} = \sum_i M_i\phi_i(t)\gamma_i^2. \tag{28}$$

Substituting equations (26)–(28) into equation (24), the Lagrange equation about the generalized coordinator $\phi_i(t)$ is simplified as follows:

$$\frac{d^2\phi_i(t)}{dt^2} + \gamma^2\phi_i(t) = \frac{Q_i(t)}{M_i}. \tag{29}$$

According to the Duhamel integral, the general solution of $\phi_i(t)$ in equation (29) can be expressed as follows:

$$\begin{aligned}\phi_i(t) = \phi_i(0)\cos\left(\gamma_i t\right) + \frac{1}{\gamma_i}\dot{\phi}_i(0)\sin\left(\gamma_i t\right)\\ + \frac{1}{\gamma_i}\int_0^t \frac{Q_i(t)}{M_i}\sin\left[\gamma_i(t-\xi)\right]d\xi.\end{aligned} \tag{30}$$

The initial conditions of $\phi_i(t)$ at zero time are as follows:

$$\begin{cases}\phi_i(0) = 0,\\ \dfrac{d\phi_i(0)}{dt} = 0.\end{cases} \tag{31}$$

Substituting equation (31) into (30), there is

$$\phi_i(t) = \frac{1}{\gamma_i}\int_0^t \frac{Q_i(t)}{M_i}\sin\left[\gamma_i(t-\xi)\right]d\xi, \tag{32}$$

where

$$\begin{aligned}Q_i(t) &= \int_0^L q(x,t)\theta_i(x)\mathrm{d}x,\\ &= \int_0^L\Bigg[q_1(t)\left[1-H(x-u(t))\right] + \left(q_2(t)+q_3(t)\right)H\left[\left(\frac{1}{2}l\right)^2 - (x-u(t))^2\right]\Bigg]\Bigg[\left(\cosh\delta_i x - \cos\delta_i x\right)\\ &\quad -\frac{\sinh\delta_i L - \sin\delta_i L}{\cosh\delta_i L + \cos\delta_i L}\left(\sinh\delta_i x - \sin\delta_i x\right)\Bigg]\mathrm{d}x.\end{aligned} \tag{33}$$

According to the properties of the Heaviside step function, the generalized force $Q_i(t)$ can be further expressed by the following equation:

$$
\begin{aligned}
Q_i(t) &= \int_0^{u(t)} q_1(t)\left[\left(\cosh\delta_i x - \cos\delta_i x\right) - \frac{\sinh\delta_i L - \sin\delta_i L}{\cosh\delta_i L + \cos\delta_i L}\left(\sinh\delta_i x - \sin\delta_i x\right)\right]\mathrm{d}x \\
&\quad + \int_{u(t)}^{u(t)+l} \left(q_2(t) + q_3(t)\right)\left(\cosh\delta_i x - \cos\delta_i x\right) - \frac{\sinh\delta_i L - \sin\delta_i L}{\cosh\delta_i L + \cos\delta_i L}\left(\sinh\delta_i x - \sin\delta_i x\right)]\mathrm{d}x \\
&= \frac{q_1(t)}{\delta_i}\left[\left(\sinh\delta_i x - \sin\delta_i x\right) - \frac{\sinh\delta_i L - \sin\delta_i L}{\cosh\delta_i L + \cos\delta_i L}\left(\cosh\delta_i x + \cos\delta_i x\right)\right]\Bigg|_0^{u(t)} \\
&\quad + \frac{q_2(t) + q_3(t)}{\delta_i}\left[\left(\sinh\delta_i x - \sin\delta_i x\right) - \frac{\sinh\delta_i L - \sin\delta_i L}{\cosh\delta_i L + \cos\delta_i L}\left(\cosh\delta_i x + \cos\delta_i x\right)\right]\Bigg|_{u(t)}^{u(t)+l}.
\end{aligned}
\tag{34}
$$

So, substituting equation (34) into equation (32), the ith-order vibration rule $\phi_i(t)$ can be achieved as follows:

$$
\phi_i(t) = \frac{1}{\gamma_i M_i \delta_i}\left(A_1 + A_2 + A_3 + A_4 + A_5 + A_6 + A_7 + A_8 + A_9\right), \tag{35}
$$

where

$$
\begin{aligned}
A_1 &= \int_0^t \left(q_1(\xi) - \left(q_2(\xi) + q_3(\xi)\right)\right)\sinh\left[\delta_i u(\xi)\right]\sin\left[\gamma_i(t-\xi)\right]d\xi, \\
A_2 &= -\int_0^t \left(q_1(\xi) - \left(q_2(\xi) + q_3(\xi)\right)\right)\sin\left[\delta_i u(\xi)\right]\sin\left[\gamma_i(t-\xi)\right]d\xi, \\
A_3 &= -n_i\int_0^t \left(q_1(\xi) - \left(q_2(\xi) + q_3(\xi)\right)\right)\cosh\left[\delta_i u(\xi)\right]\sin\left[\gamma_i(t-\xi)\right]d\xi, \\
A_4 &= -n_i\int_0^t \left(q_1(\xi) - \left(q_2(\xi) + q_3(\xi)\right)\right)\cos\left[\delta_i u(\xi)\right]\sin\left[\gamma_i(t-\xi)\right]d\xi, \\
A_5 &= \int_0^t \left(q_2(\xi) + q_3(\xi)\right)\sinh\left[\delta_i\left(u(\xi) + l\right)\right]\sin\left[\gamma_i(t-\xi)\right]d\xi, \\
A_6 &= -\int_0^t \left(q_2(\xi) + q_3(\xi)\right)\sin\left[\delta_i\left(u(\xi) + l\right)\right]\sin\left[\gamma_i(t-\xi)\right]d\xi, \\
A_7 &= -n_i\int_0^t \left(q_2(\xi) + q_3(\xi)\right)\cosh\left[\delta_i\left(u(\xi) + l\right)\right]\sin\left[\gamma_i(t-\xi)\right]d\xi, \\
A_8 &= -n_i\int_0^t \left(q_2(\xi) + q_3(\xi)\right)\cos\left[\delta_i\left(u(\xi) + l\right)\right]\sin\left[\gamma_i(t-\xi)\right]d\xi, \\
A_9 &= 2n_i\int_0^t q_1(\xi)\sin\left[\gamma_i(t-\xi)\right]d\xi, \\
n_i &= \frac{\sinh\delta_i L - \sin\delta_i L}{\cosh\delta_i L + \cos\delta_i L}.
\end{aligned}
\tag{36}
$$

Then, the vibration rule $\phi(t)$ can be calculated by performing numerical integration on equation (36). Based on the procedures presented above, the solution of equation (1) is obtained at last.

5. Results and Analysis

5.1. Physical Parameters. The detailed parameters of the armature and the rail under the laboratory conditions are shown in Table 1. The rail is made of copper, and the armature is made of aluminum. The exciting current curve is shown in Figure 5. The peak value of the current is about 400 KA at the time of 0.6 ms. Heavy pulse current with a certain pulse width can make the armature accelerate instantaneously and speed up to an extremely high level [1].

5.2. Time Varying Moving Loads. Based on the parameters listed in Table 1, the repulsive force, the contact pressure, and the thermal expansion pressure acting on the rail during launch are calculated as shown in Figures 6–8, respectively. It can be seen from Figure 6 that the repulsive force on rail always exists at the rear position of the armature as it is moving along the barrel. While in Figures 7 and 8, the contact pressure and the thermal expansion pressure only exist at the contact position between the armature and the rail. With the varying of the current, these forces change with time and reach their peaks within approximately 0.6 ms. The maximum values of the repulsive force, the contact pressure, and the thermal expansion pressure are 1.71×10^6 N/m^2, 4.08×10^6 N/m^2, and 2.24×10^8 N/m^2, respectively. It is illustrated that the thermal expansion pressure is much bigger than the repulsive force and the contact pressure. So, it is necessary to consider the thermal expansion pressure in the vibration analysis of the rail.

5.3. Movement of the Armature. When the armature is moving along the rails, the contact between the armature and the rail is seen as a sliding electrical contact. The friction coefficient of the sliding electrical contact is from 0.04 to 0.09 generally [38]. In this paper, the sliding friction coefficient is selected as 0.05. The ampere force and the friction force acting on the armature are obtained as shown in Figure 9. It can be seen that both the ampere force and the friction force are time varying. When the current reaches its peak, the forces reach their maximum values, too. The friction force is approximately 16% of the ampere force. According to the forces analysis in Section 5.2, the friction force is mainly generated by the thermal expansion force. Therefore, the armature undergoes a variable acceleration motion, whose velocity and displacement during launch are illustrated in Figure 10. It can be seen that the acceleration of the armature increases rapidly in the first half of the motion and then decreases gradually because the thrust reduces. If the initial position of the armature u_0 is assumed to be zero, the whole launch time is about 1.87 ms and the muzzle velocity of the armature is up to 1072.0 m/s.

Table 1: Parameters of the armature and the rail.

Parameter	Value
Rail length (L)	2000 mm
Rail height (h)	20 mm
Rail width (b)	10 mm
Distance between rails (s)	20 mm
Elastic modulus (E)	110 GPa
Foundation stiffness (k)	10 GPa
Contact length between armature and rail (l)	24 mm
Rail density (ρ_r)	8900 kg/m^3
Armature height (h_a)	20 mm
Armature mass (M)	20 g
Armature density (ρ_a)	2700 kg/m^3
Elastic modulus of armature (E_d)	70 GPa
Armature conductivity (σ_d)	3.7×10^7(Ω/m)
Sliding friction coefficient (μ)	0.05
Heat conduction coefficient of armature material (λ_T)	237 W/(m·°C)
Heat transfer coefficient of armature material (α_F)	500 W/(m·°C)
Linear expansion coefficient (α_T)	2.35×10^{-5} (°C^{-1})

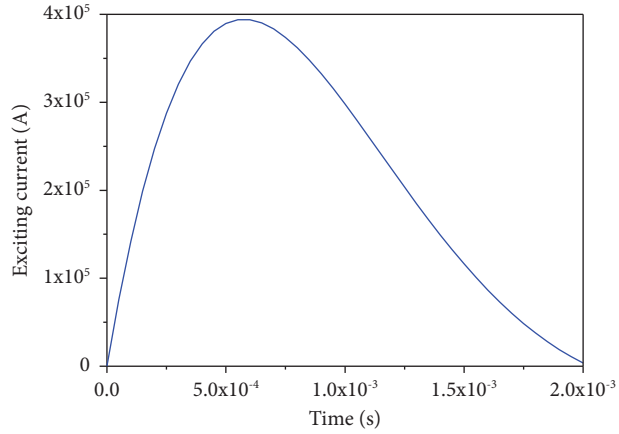

Figure 5: Curve of the exciting current.

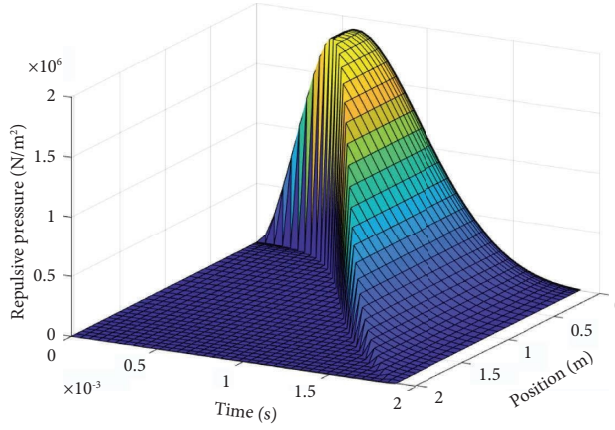

Figure 6: Repulsive force on the rail.

5.4. Vibration Response of the Rail. Based on the solving procedure presented in Section 4, the first six vibration modes of the rail are obtained as shown in Figure 11. It can

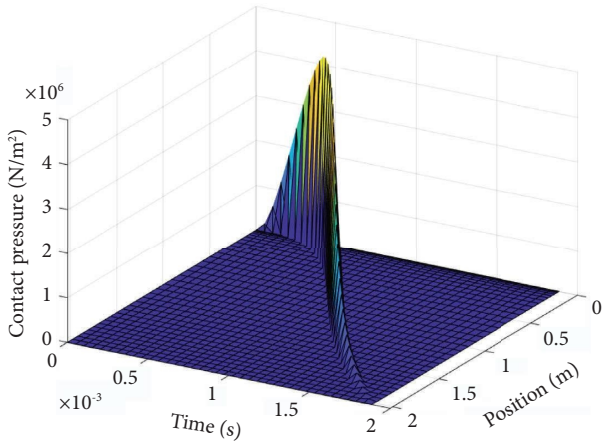

Figure 7: Contact pressure on the rail.

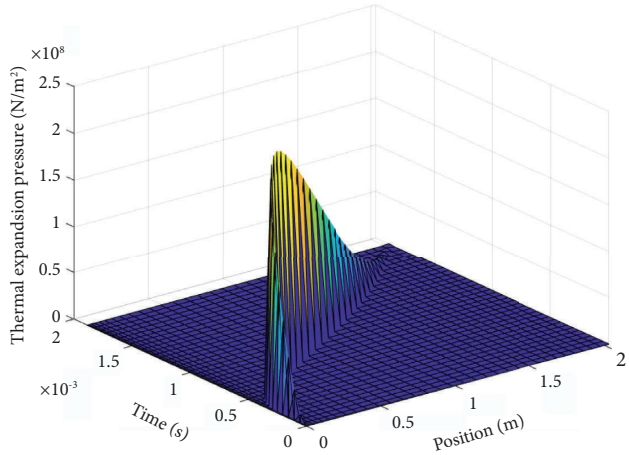

Figure 8: Thermal expansion pressure on the rail.

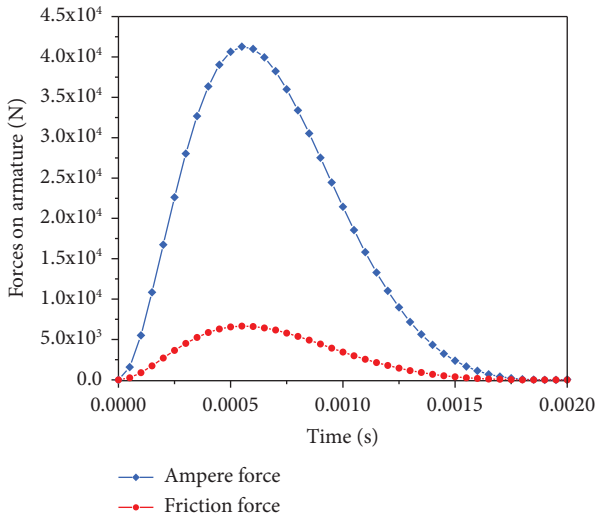

Figure 9: Forces on the armature.

be seen that as the mode order increases, the natural frequency increases. Using high-order modes to calculate the vibration response of the rail can improve the calculation

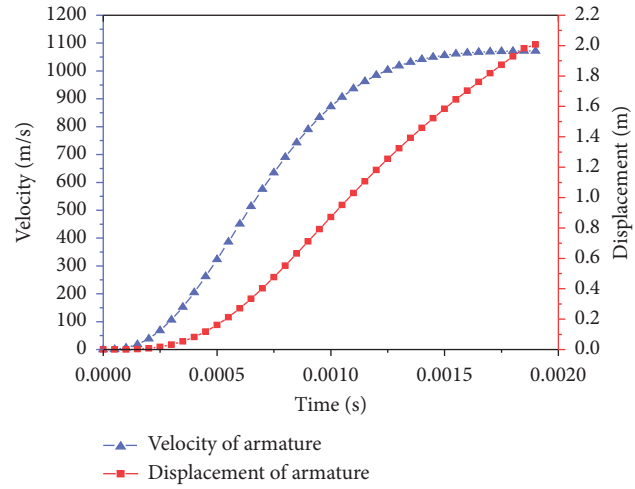

Figure 10: Velocity and displacement of the armature during launch.

accuracy, but the calculation cost is high. According to the vibration mechanics theory, the vibration of a beam is mainly affected by low-order modes. So, the first three order modes are used for the calculation of vibration amplitudes [39].

The vibration response of the rail under time varying moving loads is shown in Figure 12. As the armature moves along the rail, the dynamic response of the rail at different times and positions can be obtained from the graph. It can be seen from Figure 12 that the rail vibration is low frequency deflection wave. This tendency agrees with the results obtained in reference [14], approximately. When the deflection is positive, it means that the railgun caliber is constricted [14]. In Figure 12, the vibration amplitude at the middle of the rail is obviously larger than that at other locations. When the armature runs for 1.1 ms and reaches the position of 0.983 m of the rail, the maximum vibration amplitude (MVA) of the rail is about 1.79×10^{-4} m. The MVAs at different positions of the rail are different during the period of launch. From a local perspective, the MVAs at the positions of 0.8 m, 1.0 m, and 1.2 m of the rail are 1.72×10^{-4} m, 1.78×10^{-4}m, and 1.33×10^{-4} m, respectively, as given in Figure 13.

5.5. Effects of Parameters on Lateral Vibration

5.5.1. Elastic Foundation Coefficient. The elastic foundation coefficient of the supporting structure is an important parameter, which will affect the lateral vibration amplitude of the rail. But the armature motion will not be affected because the exciting current and the geometric structure parameters of the rail are unchanged.

Now, the elastic foundation coefficient is set to be 7 GPa, 10 GPa, and 15 GPa, respectively. The lateral vibration amplitudes at the position of 1.0 m are shown in Figure 14. It can be seen that the MVA of the rail decreases with the increasing of the elastic foundation stiffness. When the elastic foundation coefficients are 7 GPa, 10 GPa, and 15 GPa, the MVAs are 2.55×10^{-4} m, 1.78×10^{-4} m, and

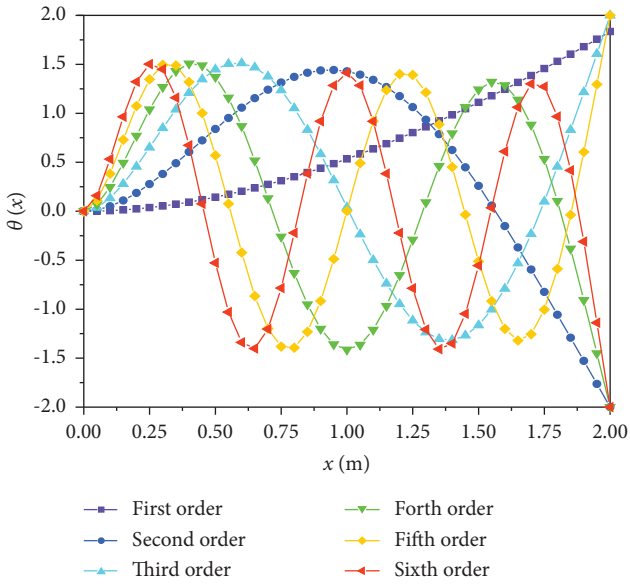

Figure 11: First six vibration modes of the rail.

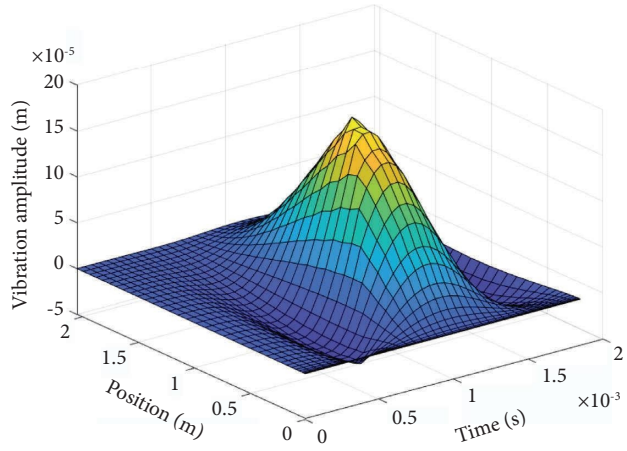

Figure 12: Lateral vibration amplitude versus time and position of the rail.

1.17×10^{-4} m, respectively. Therefore, to reduce the vibration amplitude of the rail, the elastic foundation stiffness should be enhanced as much as possible by changing the foundation material or dimensions.

5.5.2. Rail Width. When the rail width is varied, the magnetic induction intensity and the inductance gradient as well as the moment of inertia of the rail will change correspondingly. Here, the rail widths of 8 mm, 10 mm, and 12 mm are selected for calculation. The moment of inertia, the inductance gradient, and the magnetic induction intensity under different widths are calculated, as listed in Table 2. It can be seen that when the rail width increases, the moment of inertia increases, and the bending stiffness of the rail is enhanced. However, the inductance gradient and the magnetic induction intensity decrease slightly, and it means that the forces acting on the rail will get smaller.

The velocity and the displacement of the armature under different rail widths are given in Figures 15 and 16. It can be seen that the running speed of the armature decreases with the increasing of the rail width. When the rail widths are 8 mm, 10 mm, and 12 mm, the muzzle velocities of the armature are 1085.1 m/s, 1072.0 m/s, and 1056.9 m/s, respectively. Correspondingly, the running times of the armature on the 2-meter long rail are 1.81 ms, 1.87 ms, and 1.93 ms, respectively.

Then, the lateral vibration amplitudes at 1.0 m of the rail are shown in Figure 17. It can be seen that the vibration amplitude of the rail decreases with the increasing of the width of the rail. When the rail widths are 8 mm, 10 mm, and 12 mm, the MVAs are 1.89×10^{-4} m, 1.78×10^{-4} m, and 1.62×10^{-4} m, respectively.

5.5.3. Rail Height. Here, the rail heights of 18 mm, 20 mm, and 22 mm are selected for calculation. The moment of inertia, the inductance gradient, and the magnetic induction intensity under different heights are calculated as listed in Table 3. It can be seen that when the rail height increases, the moment of inertia increases, while the inductance gradient and the magnetic induction intensity decrease.

The velocity and the displacement of the armature under different rail heights are given in Figures 18 and 19. It is illustrated that the running speed of the armature decreases with the increasing of the rail height. When the rail heights are 18 mm, 20 mm, and 22 mm, the muzzle velocities of the armature are 1079.2 m/s, 1072.0 m/s, and 1065.9 m/s, respectively. Correspondingly, the running times of the armature on the 2-meter long rail are 1.85 ms, 1.87 ms, and 1.90 ms.

Then, the lateral vibration amplitudes at 1.0 m of the rail are shown in Figure 20. It can be seen that the lateral vibration amplitude of the rail decreases with the increasing of the rail height. When the rail heights are 18 mm, 20 mm, and 22 mm, the MVAs are 2.19×10^{-4} m, 1.78×10^{-4} m, and 1.46×10^{-4} m, respectively.

Now, in order to compare the effects of different factors on the muzzle velocity of the armature and the MVA of the rail, the relative reduction rates are listed in Table 4. The relative reduction rate R_i is computed by the following equation:

$$R_i = \frac{D_i - D_1}{D_1} \times 100\%, \tag{37}$$

where D_1 is the first data and D_i ($i = 2, \ldots, m$) represents the other data.

It can be seen from Table 4 that the changing of parameters has a little effect on the muzzle velocity of the armature, but an obvious effect on the MVA of the rail. Relatively speaking, the influences of the rail height and the elasticity foundation stiffness are greater than that of the rail width. Among them, the relative reduction rate of the MVA reaches 54.2% when the foundation elastic stiffness increases to 15 GPa, and the relative reduction rate of the MVA reaches 33.3% when the rail height increases to 22 mm.

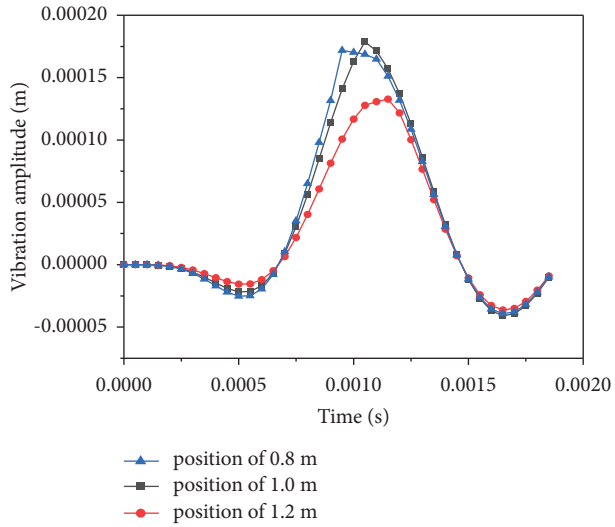

Figure 13: Curves of vibration amplitude versus time at different positions of the rail.

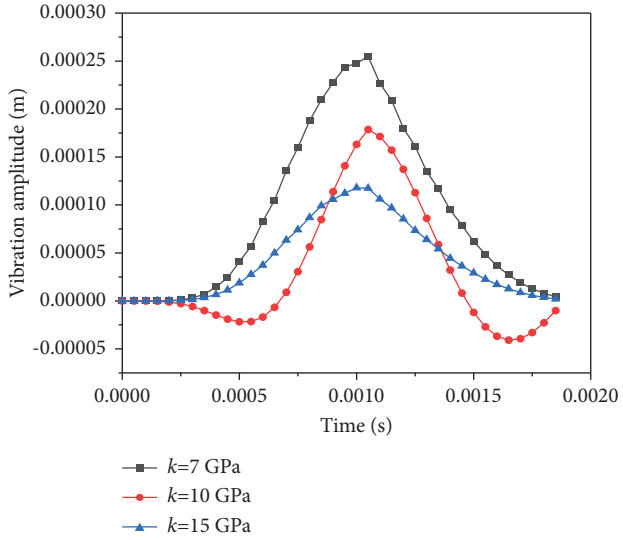

Figure 14: Effects of the elastic foundation coefficient on the lateral vibration of the rail.

Table 2: Mechanical parameters under different rail widths.

Rail width, b (mm)	Moment of inertia, I (mm^4)	Inductance gradient, L' (μH/m)	Magnetic induction intensity, B (T)
8	853.3	0.4901	12.76
10	1666.7	0.4860	12.65
12	2880.0	0.4813	12.19

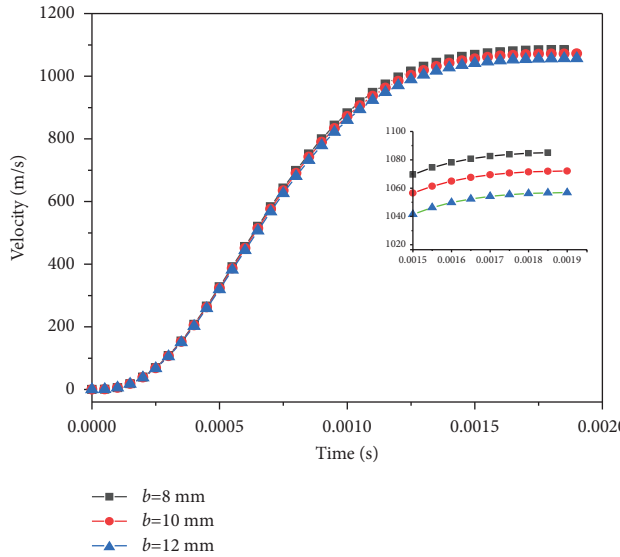

Figure 15: Velocities of the armature under different widths of the rail.

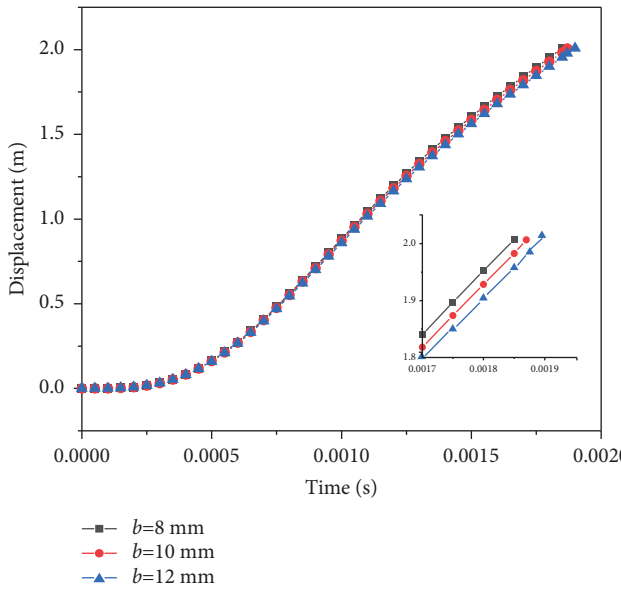

Figure 16: Displacements of the armature under different widths of the rail.

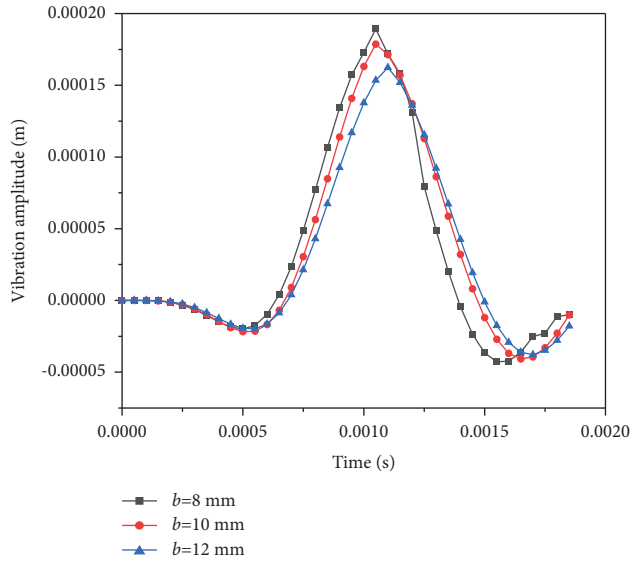

Figure 17: Effects of rail widths on the lateral vibration of the rail.

Table 3: Mechanical parameters under different rail heights.

Rail height, h (mm)	Moment of inertia, I (mm^4)	Inductance gradient, L' (μH/m)	Magnetic induction intensity, B (T)
18	1500.0	0.4881	13.25
20	1666.7	0.4860	12.65
22	1833.3	0.4840	12.05

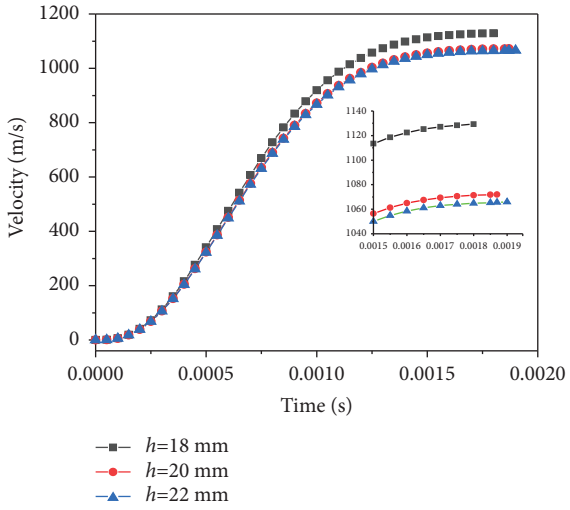

Figure 18: Velocities of the armature under different heights of the rail.

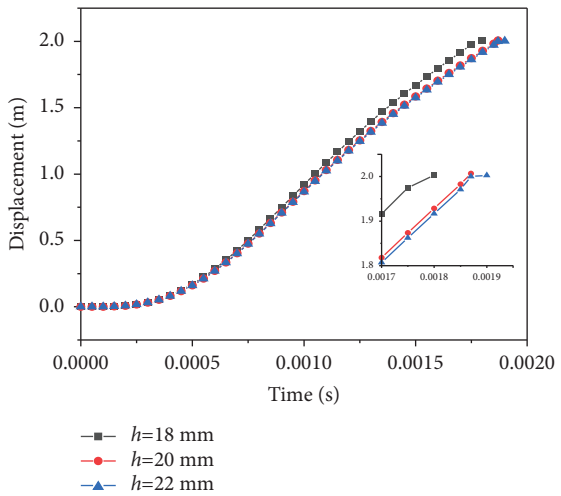

Figure 19: Displacements of the armature under different heights of the rail.

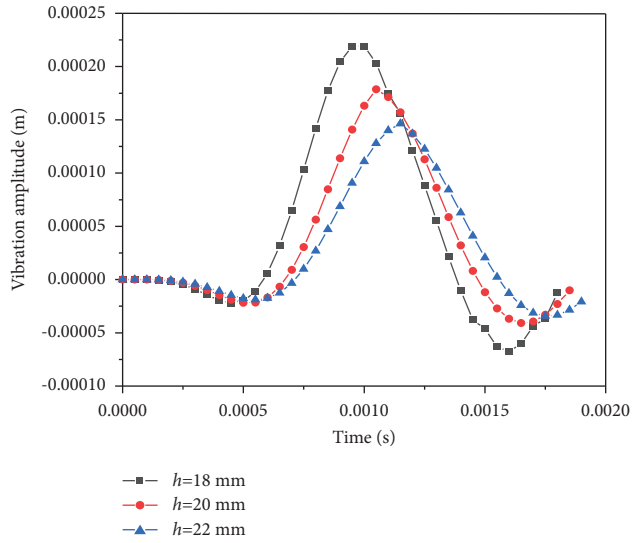

Figure 20: Effects of rail heights on lateral vibration of the rail.

Table 4: Summary of results for comparison.

Parameter	Foundation stiffness, k (GPa)			Rail width, b (mm)			Rail height, h (mm)		
Value	7	10	15	8	10	12	18	20	22
Muzzle velocity (m/s)	1072.0	1072.0	1072.0	1085.1	1072.0	1056.9	1079.2	1072.0	1065.9
Relative reduction rate	0	0	0	0	1.2%	2.6%	0	0.7%	1.2%
Maximum vibration amplitude ($\times 10^{-4}$ m)	2.55	1.78	1.17	1.89	1.78	1.62	2.19	1.78	1.46
Relative reduction rate	0	30.2%	54.1%	0	5.8%	14.3%	0	18.7%	33.3%

6. Conclusions

In this paper, an analytical method combined with numerical integration is proposed to investigate the lateral vibration of rails under time varying moving loads. The dynamic response of the simplified Euler–Bernoulli beam is obtained. The main results are as follows:

(1) A dynamic analysis of an EM rail under time varying moving load is carried out based on the Winkler model by using the method of separation of variables and the Lagrange procedure. An intuitive 3D graph reflecting the change of rail vibration with launch time and rail position is achieved. It can be seen that the lateral vibration pattern mainly appears as

deviation from the axis of the railgun bore. The vibration amplitude at the middle position of the rail is much bigger than that at other locations. The maximum vibration amplitude can reach 1.79×10^{-4} m. This provides an idea for the structure design of the rail, i.e., an irregular section rail with high stiffness in its middle part is needed to reduce the vibration amplitude of the rail.

(2) The time for the armature to pass through a 2-meter long rail is approximately 1.8 ms. The muzzle velocity of the armature is about 1043 m/s. During the whole launch time, the time varying forces reach their peaks when the current is biggest at 0.6 ms. The thermal expansion pressure induced by the Joule heating effect at the contact area between the armature and the rail is much bigger than the repulsive force and the contact pressure. It is about a hundred times that of the repulsive force. So, it is the main cause of friction and wear between the armature and the rail.

(3) The vibration response is influenced by the dimensions of the rail and the brace stiffness obviously. Increasing the width and the height of the rail and the elastic foundation stiffness can reduce the vibration magnitude. Relatively speaking, the relative reduction rates of the MVAs obtained by increasing the foundation stiffness and the rail height are bigger than that obtained by increasing the rail width. The relative reduction rate reaches 54.2% by increasing the foundation stiffness from 7 GPa to 15 GPa and 33.3% by increasing the rail height from 18 mm to 22 mm. It should be noted that although the relative reduction rate is significantly higher, it is difficult to enhance the foundation stiffness to such a high level. Therefore, it is advisable to increase the rail height as a priority for vibration reduction. In addition, it is good to see that the variation of parameters has slight effects on the muzzle velocity of the armature.

Next, further works will be conducted on the forces and dynamic responses of irregular rails (with concave or convex cross-section) of EM railguns, as well as the variable cross section rails like the trapezoidal rail. The aim is to study the effects of rail beams with special shapes on the vibration reduction of EM railguns. Moreover, it is necessary to investigate the influence of the rail vibration on the shot accuracy of EM railguns in the future.

Appendix

A. Details of Solving Coefficients in Equation (21) under Boundary Conditions

The aim of this procedure is to obtain the coefficients a_j ($j = 1, \ldots, 4$) of the following equation:

$$\theta(x) = a_1 \sinh \delta x + a_2 \cosh \delta x + a_3 \sin \delta x + a_4 \cos \delta x. \tag{A.1}$$

According to the simplified beam model of the rail, both the deflection and rotation angle of the fixed end are zero, and the bending moment and shear stress of the free end are also zero. Hence, when the length of the rail is L, its boundary conditions are as follows:

$$x = 0: \begin{cases} \theta(x) = 0, \\ \dfrac{d\theta(x)}{dx} = 0, \end{cases} \quad \text{and } x = L: \begin{cases} \dfrac{d^2\theta(x)}{dx^2} = 0, \\ \dfrac{d^3\theta(x)}{dx^3} = 0. \end{cases} \tag{A.2}$$

Substituting equation (A.2) into equation (A.1), the following relations are obtained:

$$\begin{aligned} \theta(0) &= a_2 + a_4 = 0, \\ \left(\frac{d\theta(x)}{dx}\right)\Big|_{x=0} &= \delta(a_1 + a_3) = 0, \end{aligned} \tag{A.3}$$

$$\begin{aligned} \left(\frac{d^2\theta(x)}{dx^2}\right)\Big|_{(x=L)} &= \delta^2 (a_1 \sinh \delta L + a_2 \cosh \delta L - a_3 \sin \delta L - a_4 \cos \delta L) = 0, \\ \left(\frac{d^3\theta(x)}{dx^3}\right)\Big|_{(x=L)} &= \delta^3 (a_1 \cosh \delta L + a_2 \sinh \delta L - a_3 \cos \delta L + a_4 \sin \delta L) = 0. \end{aligned} \tag{A.4}$$

It can be seen from equations (A.3) and (A.4) that there must be the following relations to have nonzero a_1 and a_2:

$$\begin{vmatrix} \sinh \delta L + \sin \delta L & \cosh \delta L + \cos \delta L \\ \cosh \delta L + \cos \delta L & \sinh \delta L - \sin \delta L \end{vmatrix} = 0. \tag{A.5}$$

So, we can obtain the following equation:

$$\cosh \delta L \cdot \cos \delta L + 1 = 0. \tag{A.6}$$

According to the boundary conditions, when the value of a_2 is set to 1, the constants a_1, a_3, and a_4 are obtained as follows:

$$a_1 = -a_3 = \frac{\sinh\delta_i L - \sin\delta_i L}{\cosh\delta_i L + \cos\delta_i L},$$
$$a_4 = -a_2 = -1, \tag{A.7}$$

where $\delta_i = (i-0.5)\pi/L$, $(i = 1, 2...n)$ and n represents the number of modes.

B. Details of Solving the Kinetic Energy and the Total Potential Energy of the Beam

The kinetic energy of the beam T is expressed as follows:

$$T = \frac{1}{2}\int_0^L m\left(\frac{\partial\omega(x,t)}{\partial t}\right)^2 \mathrm{d}x. \tag{B.1}$$

Then, substituting equation (14) into equation (B.1), there is

$$T = \frac{1}{2}\sum_i\sum_j \frac{d\phi_i(t)}{dt}\frac{d\phi_j(t)}{dt}\int_0^L m\theta_i(x)\theta_j(x)\mathrm{d}x. \tag{B.2}$$

Combining equation (B.2) with equation (23), the kinetic energy of the beam T can be obtained as follows:

$$T = \frac{1}{2}\sum_i M_i\left(\frac{d\phi_i(t)}{dt}\right)^2, \tag{B.3}$$

where M_i represents the generalized mass of the beam, which is expressed as follows:

$$M_i = \int_0^L m\theta_i^2(x)\mathrm{d}x. \tag{B.4}$$

In addition, the total potential energy is determined by the strain energy of the rail and the strain energy of the elastic foundation.

The strain energy of the rail $\mathbf{U_s}$ is computed by the following equation:

$$U_s = \frac{1}{2}\int_0^L \mathrm{EI}\left(\frac{\partial^2\omega(x,t)}{\partial t^2}\right)^2 dx = \frac{1}{2}\sum_i\sum_j \phi_i(t)\phi_j(t)\int_0^L \mathrm{EI}\frac{d^2\theta_i(x)}{dx^2}\frac{d^2\theta_j(x)}{dx^2}dx = \frac{1}{2}\frac{\mathrm{EI}}{m}\sum_i \delta_i{}^4 M_i\phi_i{}^2(t). \tag{B.5}$$

Also, the strain energy of the elastic foundation $\mathbf{U_b}$ is computed by the following equation:

$$U_b = \frac{1}{2}\int_0^L k\omega^2(x,t)dx = \frac{1}{2}k\int_0^L\left(\sum_i \theta(x)\phi(t)\right)^2 dx = \frac{k}{2}\sum_i\sum_j \phi_i(t)\phi_j(t)\int_0^L \theta_i(x)\theta_j(x)dx = \frac{k}{2m}M_i\sum_i \phi_i{}^2(t). \tag{B.6}$$

Thus, the total potential is achieved as follows:

$$U = U_s + U_b = \frac{1}{2}\frac{EI}{m}\sum_i \delta_i{}^4 M_i\phi_i{}^2(t) + \frac{k}{2m}M_i\sum_i \phi_i{}^2(t) = \frac{1}{2}\sum_i M_i\phi_i{}^2(t)\gamma_i^2. \tag{B.7}$$

Data Availability

The data used to support the findings of the study are included in the paper.

Conflicts of Interest

The authors declare that they have no conflicts of interest.

References

[1] Z. Z. Su, W. Guo, and T. Zhang, *Technology of Electromagnetic Railguns*, National Defence Industry Press, Beijing, 2019.

[2] I. R. McNab, F. Stefani, M. Crawford et al., "Development of a naval railgun," *IEEE Transactions on Magnetics*, vol. 41, no. 1, pp. 206–210, 2005.

[3] N. Doerry, J. Amy, and C. Krolick, "History and the status of electric ship propulsion, integrated power systems, and future trends in the U.S. navy," *Proceedings of the IEEE*, vol. 103, no. 12, pp. 2243–2251, 2015.

[4] M. F. Stumborg, "The impact of gun dimensions on the operational effectiveness of a Naval surface fleet equipped with long range electromagnetic guns," *IEEE Transactions on Magnetics*, vol. 37, no. 1, pp. 498–501, 2001.

[5] W. M. Ma and J. Y. Lu, "Thinking and study of electromagnetic launch technology," *IEEE Transactions on Plasma Science*, vol. 45, no. 7, pp. 1071–1077, 2017.

[6] A. J. Johnson, T. Haran, F. C. Moon, and W. Robinson, "Stress wave measurements in an electroma-gnetic launcher," in *Proceedings of 14th International Symposium on Electromagnetic Launch Techn-ology*, pp. 10–13, Victoria, BC, Canada, June 2008.

[7] J. T. Tzeng, "Dynamic response of electromagnetic railgun due to projectile movement," *IEEE Transactions on Magnetics*, vol. 39, no. 1, pp. 472–475, 2003.
[8] J. T. Tzeng, "Structural mechanics for electromagnetic railguns," *IEEE Transactions on Magnetics*, vol. 41, no. 1, pp. 246–250, 2005.
[9] A. J. Johnson and F. C. Moon, "Elastic waves and solid armature contact pressure in electromagnetic launchers," *IEEE Transactions on Magnetics*, vol. 42, no. 3, pp. 422–429, 2006.
[10] N. V. Nechitailo and K. B. Lewis, "Critical velocity for rails in hypervelocity launchers," *International Journal of Impact Engineering*, vol. 33, no. 1-12, pp. 485–495, 2006.
[11] N. V. Nechitailo and K. B. Lewis, "Influence of the critical velocity on deformation of launcher components," *International Journal of Impact Engineering*, vol. 35, no. 12, pp. 1683–1687, 2008.
[12] K. Daneshjoo, M. Rahimzadeh, R. Ahmadi, and M. Ghassemi, "Dynamic response and armature critical velocity studies in an electromagnetic railgun," *IEEE Transactions on Magnetics*, vol. 43, no. 1, pp. 126–131, 2007.
[13] L. Yang, J. X. Nie, and M. Ren, "Dynamic characteristics of armature and rail with cambered surface under moving electromagnetic load," *High Voltage Engineering*, vol. 40, no. 4, pp. 1091–1096, 2014.
[14] B. Reck, S. Hundertmark, G. Vincent, F. Schubert, and M. Schneider, "Investigation of rail deformation and stress wave propagation in the ISL-NGL60 Railgun," *IEEE Transactions on Plasma Science*, vol. 47, no. 5, pp. 2556–2559, 2019.
[15] T. N. Chen, C. Y. Bai, and Y. N. Zhang, "Dynamic response of electromagnetic railgun due to armature movement," *Journal of Dynamics and Control*, vol. 8, pp. 360–364, 2010.
[16] Z. G. Tian, X. Z. Bai, and Y. Yang, "Dynamic response of rail under a launching state of an electromagnetic rail," *Journal of Vibration and Shock*, vol. 31, no. 2, pp. 10–14, 2012.
[17] D. M. Yin, H. C. Xiao, and B. M. Li, "Dynamics response of filament-wound composite barrel for rail gun with acceleration load," *IEEE Transactions on Plasma Science*, vol. 46, no. 5, pp. 1847–1854, 2018.
[18] B. Zhang, Y. Kou, K. Jin, and X. Zheng, "Dynamic response of electromagnetic railgun under time-dependent electromagnetic moving loads," *Journal of Sound and Vibration*, vol. 483, Article ID 115451, 2020.
[19] R. AlSaleh, A. Nasir, and I. Abu-Alshaikh, "Investigating fractional damping effect on Euler-Bernoulli beam subjected to a moving load," *Shock and Vibration*, vol. 2023, Article ID 9524177, pp. 1–19, 2023.
[20] Ş. D. Akbaş, S. Dastjerdi, B. Akgoz, and O. Civalek, "Dynamic analysis of functionally graded porous microbeams under moving load," *Transport in Porous Media*, vol. 142, no. 1-2, pp. 209–227, 2022.
[21] S. D. Akbas, H. M. Numanoglu, B. Akgoz, and O. Civalek, "Application of newmark average accele-ration and Ritz methods on dynamical analysis of composite beams under a moving load," *Journal of Applied and Computational Mechanics*, vol. 8, no. 2, pp. 764–773, 2022.
[22] L. Guo, X. Y. Xin, D. Shahsavari, and B. Karami, "Dynamic response of porous E-FGM thick microp- late resting on elastic foundation subjected to moving load with acceleration," *Thin-Walled Structures*, vol. 173, Article ID 108981, 2022.
[23] B. Bozyigit, "Dynamic response of damaged rigid-frame bridges subjected to moving loads using ana-lytical based formulations," *Engineering Computations*, vol. 40, no. 4, pp. 793–822, 2023.
[24] C. S. Kumar, C. Sujatha, and K. Shankar, "Vibration of simply supported beams under a single moving load: a detailed study of cancellation phenomenon," *International Journal of Mechanical Sciences*, vol. 99, pp. 40–47, 2015.
[25] I. Esen, "Dynamics of size-dependant Timoshenko micro beams subjected to moving loads," *International Journal of Mechanical Sciences*, vol. 175, Article ID 105501, 2020.
[26] A. Eyvazian, D. Shahsavari, and B. Karami, "On the dynamic of graphene reinforced nanocomposite cylindrical shells subjected to a moving harmonic load," *International Journal of Engineering Science*, vol. 154, Article ID 103339, 2020.
[27] S. M. Kim and Y. H. Cho, "Vibration and dynamic buckling of shear beam- columns on elastic foun-dation under moving harmonic loads," *International Journal of Solids and Structures*, vol. 43, no. 3-4, pp. 393–412, 2006.
[28] Y. B. Yang, K. Shi, X. Q. Mo, Z.-L. Wang, H. Xu, and Y. T. Wu, "Internal instability of thin-walled beams under harmonic moving loads," *Thin-Walled Structures*, vol. 174, Article ID 109123, 2022.
[29] J. S. Chen, Q. W. Wen, and C. Yeh, "Steady state responses of an infinite beam resting on a tensionle-ss visco-elastic foundation under a harmonic moving load," *Journal of Sound and Vibration*, vol. 540, Article ID 117298, 2022.
[30] B. Bozyigit, Y. Yesilce, and S. Catal, "Free vibrations of axial-loaded beams resting on viscoelastic foundation using adomian decomposition method and differential transformation," *Engineering Science and Technology, an International Journal*, vol. 21, no. 6, pp. 1181–1193, 2018.
[31] B. Cao, X. Ge, W. Guo et al., "Analysis of rail dynamic deformation during electromagnetic launch," *IEEE Transactions on Plasma Science*, vol. 45, no. 7, pp. 1269–1273, 2017.
[32] J. G. Wu, Q. H. Lin, and B. M. Jia, "Dynamic response analysis of conducting rails in electromagnetic rail launcher," *Journal of Vibration Engineering*, vol. 32, pp. 120–127, 2019.
[33] L. Z. Xu and Y. B. Geng, "Forces of rails for electromagnetic railguns," *Applied Mathematical Modelling*, vol. 36, no. 4, pp. 1465–1476, 2012.
[34] M. J. Siopis and R. W. Neu, "Wear at high sliding speeds and high contact pressures," *Wear*, vol. 342-343, pp. 356–363, 2015.
[35] J. X. Nie, J. J. Han, Q. J. Jiao, J. Li, and J. F. Qin, "An analytic expression of inductance gradient for rail-type electromagnetic launcher," *IEEE Transactions on Plasma Science*, vol. 39, no. 3, pp. 931–934, 2011.
[36] M. A. Мичеев, *Fundamentals of Heat Transfer*, Higher Education Press, Beijing, 1985.
[37] S. D. Akbas, H. Ersoy, B. Akgoz, and O. Civalek, "Dynamic analysis of a fiber reinforced composite beam under a moving load by the Ritz method," *Mathematics*, vol. 9, no. 1048, pp. 1–11, 2021.
[38] F. Y. Guo and Z. H. Chen, *Electrical Contact Theory and its Applications*, China power press, Beijing, 2008.
[39] D. S. Wang, *Theory of Gun Vibration*, Weapon Industry Press, Beijing, 2015.